

Structure of end states for a Haldane Spin Chain

M. Kenzelmann^{1,2}, G. Xu,³ I. A. Zaliznyak,³ C. Broholm^{1,2},
J. F. DiTusa,⁴ G. Aeppli,^{5,6} T. Ito,⁷ K. Oka⁷ and H. Takagi⁸

- (1) Department of Physics and Astronomy, Johns Hopkins University, Baltimore, Maryland 21218
(2) NIST Center for Neutron Research, National Institute of Standards and Technology, Gaithersburg, Maryland 20899
(3) Department of Physics, Brookhaven National Laboratory, Upton, New York 11973-5000
(4) Department of Physics and Astronomy, Louisiana State University, Baton Rouge, Louisiana 70803
(5) London Centre for Nanotechnology, Gower Street, London WC1E 6BT, UK
(6) NEC Research Institute, 4 Independence Way, Princeton, New Jersey 08540
(7) National Institute of Advanced Industrial Science and Technology, Tsukuba, Ibaraki 305-8562, Japan
(8) Graduate School of Frontier Sciences, University of Tokyo, Hongo, Bunkyo-ku, Tokyo 113-8656, Japan
(Dated: November 7, 2018)

Inelastic neutron scattering was used to probe edge states in a quantum spin liquid. The experiment was performed on finite length antiferromagnetic spin-1 chains in $Y_2BaNi_{1-x}Mg_xO_5$. At finite fields, there is a Zeeman resonance below the Haldane gap. The wave vector dependence of its intensity provides direct evidence for staggered magnetization at chain ends, which decays exponentially towards the bulk ($\xi = 8(1)$ at $T = 0.1$ K). Continuum contributions to the chain end spectrum indicate inter-chain-segment interactions. We also observe a finite size blue shift of the Haldane gap.

PACS numbers: 75.25.+z, 75.10.Jm, 75.40.Gb

Highly-correlated electron systems can have quantum ground states that are coherent over macroscopic length scales. Among the best known examples is the two-dimensional electron gas in a magnetic field where Coulomb interactions lead to cooperative excitations with fractional charge as evidenced in the quantum Hall effect. Spin systems with strong quantum fluctuations feature similar cooperative phenomena with coherent spin excitations that differ fundamentally from classical spin waves.

Impurities and boundaries can liberate novel composite degrees of freedom and dramatically change the physical properties of macroscopic quantum systems. Spin correlations in the vicinity of impurities are of particular interest because they reflect the nature of the underlying bulk quantum state, and because they may be important for understanding unconventional bulk properties. Many recent experiments have therefore been carried out to probe the effects of impurities on quantum fluids. For example, scanning tunnelling microscopy and NMR have examined the response of high-temperature superconductors to Zn, Ni and Li substituted for Cu atoms [1, 2], while neutron scattering has revealed that holes create AF droplets with a central π phase shift in the one-dimensional Haldane spin liquid [3].

In this Letter we present direct information about vacancy-induced edge states in the one-dimensional (1D) $S=1$ Heisenberg antiferromagnet (AF) $Y_2BaNi_{1-x}Mg_xO_5$ obtained through a novel inelastic neutron scattering technique. The relative simplicity of a 1D $S=1$ antiferromagnet allows straightforward interpretation of the data, and therefore can serve as a step toward understanding impurity-induced phenomena in more complicated systems. The Hamiltonian for an

AF spin chain is

$$\mathcal{H} = J \sum_i \mathbf{S}_i \mathbf{S}_{i+1}, \quad (1)$$

where $J > 0$ is the nearest-neighbor exchange constant. For $S=1$ the ground state of Eq. 1 is an isolated singlet in which correlations fall off exponentially and the excitation spectrum has an energy gap [4]. The ground state is similar to that of the Affleck-Kennedy-Leib-Tasaki (AKLT) model [5], where the $S=1$ states are described as two $S=\frac{1}{2}$ states and the ground state is made up of local AF valence bonds between $S=\frac{1}{2}$ states of nearest-neighbor sites. The first excited state corresponds to breaking a valence bond singlet, hence the gap.

Non-magnetic impurities in $S=1$ chains should produce an ensemble of finite length chain segments with a singlet-triplet gap that increases with decreasing chain length [6] as well as localized $S=\frac{1}{2}$ degrees of freedom at chain ends [5]. The strongest evidence for $S=\frac{1}{2}$ degrees of freedom from non-magnetic doping was obtained through ESR [7] and NMR [8] experiments. It is important to note, though, that in real $S=1$ chains, we are dealing with *effective* $S=\frac{1}{2}$ degrees of freedom, which always occur in $S=0$ and $S=1$ pairs, a fact graphically illustrated by magnetic specific heat data [9]. Here we present inelastic neutron scattering experiments which probe the microscopic structure of the chain end states through the wave-vector dependence of the Zeeman resonance.

Y_2BaNiO_5 has a body-centered orthorhombic structure, space group $Immm$ with lattice parameters $a = 3.76 \text{ \AA}$, $b = 5.76 \text{ \AA}$ and $c = 11.32 \text{ \AA}$ [10]. The Ni^{2+} chains run along the a -axis and the Ni^{2+} ions are separated by \mathbf{a} , so $\mathbf{Q}=(h, k, l)=(0.5, 0, 0)$ is the AF point, which is also referred to as the $q = \pi$ -point in theoretical

work. The samples were grown by the travelling-solvent floating-zone method [11]. The experiments were performed at the NIST Center for Neutron Research.

The excitation spectrum of AF $S=1$ chains near AF wave-vectors is dominated by well-defined triplet excitations with an energy gap $\Delta = 0.41050(2)J$ [6]. Open circles in Fig. 1 show the spectrum of the nominally pure sample, Y_2BaNiO_5 , at the AF point $q = \pi$, measured at $(0.5, 1.5, 0)$. A non-magnetic background, determined by matching constant- \mathbf{Q} scans with the sample offset by 20° , was subtracted from the data. Crystal field anisotropies in Y_2BaNiO_5 split the Haldane triplet into three separate modes at 7.5(1), 8.6(1) and 9.6(1) meV for polarizations parallel to the three principal orthorhombic axes [12]. The experiment at $(0.5, 1.5, 0)$ is least sensitive to $S^{bb}(\mathbf{Q}, \omega)$ because neutron scattering probes the dynamic spin correlation functions of spin components perpendicular to the wave-vector transfer \mathbf{Q} :

$$\frac{d^2\sigma(\mathbf{Q}, \omega)}{d\Omega dE_f} = \frac{k_f}{k_i} \left(\frac{g}{2} F_{\text{Ni}}(\mathbf{Q})\right)^2 \sum_{\alpha\beta} (1 - \hat{Q}_\alpha \hat{Q}_\beta) S^{\alpha\beta}(\mathbf{Q}, \omega). \quad (2)$$

Here $F_{\text{Ni}}(\mathbf{Q})$ is the magnetic form factor of Ni^{2+} .

Closed circles in Fig. 1 show the spectrum for the doped sample, $\text{Y}_2\text{BaNi}_{0.96}\text{Mg}_{0.04}\text{O}_5$, measured at the same wave-vector and under similar resolution conditions. In agreement with work on powder samples of $\text{Y}_2\text{BaNi}_{0.96}\text{Zn}_{0.04}\text{O}_5$ [13], the spectrum is attenuated and harder than in the undoped sample, even though the threshold and peak energies remain essentially the same. This follows because there is now a distribution of chain lengths with the Haldane gap rising with decreasing chain length. The longest chains contribute unchanged spectra and threshold energies, while the shorter chain spectra are (blue) shifted to higher energies and produce the enhanced - relative to the peak - high frequency tail.

Indeed the observed neutron spectra follow quantitatively from the random distribution of the non-magnetic defects in the sample. For defect density, x , the probability that $L + 2$ sites form an isolated chain segment of length L is $P(L, x) = x^2(1-x)^L$. Numerical calculations suggest that the energy gap in a chain of length L is $\Delta^\alpha(L) = \sqrt{(\Delta_\infty^\alpha)^2 + v_s^2 \cdot \sin^2(\pi(1-1/L))}$ [6], where $v_s = 2.49(1)J$ is the spin-wave velocity [14]. The average dynamical structure factor is then given by $S(\mathbf{Q}, \omega) = \sum_L P(L) S_L(\mathbf{Q}, \omega)$, where $S_L(\mathbf{Q}, \omega)$ is the structure factor for a chain segment of length L . For simplicity we chose $S_L(\mathbf{Q}, \omega)$ to equal that for an infinite length chain suitably normalized so as to correspond to L spin and with gap $\Delta(L)$ [15]. $S(\mathbf{Q}, \omega)$ was convoluted with the resolution function [16] and adjusted to the data in a global fit. The fit for the nominally pure sample included a residual impurity concentration, $x = 0.010(1)$, that was determined from the Curie tail in low- T susceptibility data [12]. For the doped sample the impurity concentra-

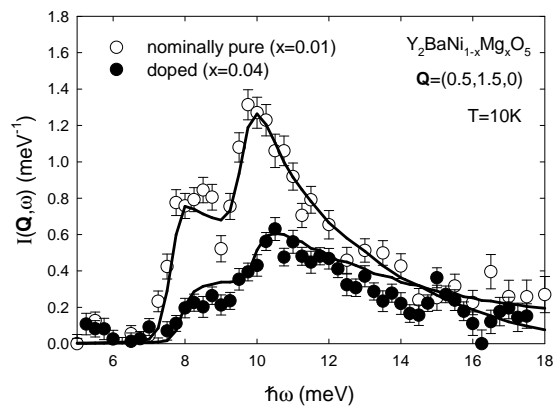


FIG. 1: Scattering spectra at $(0.5, 1.5, 0)$ for doped and undoped Y_2BaNiO_5 , shown in absolute units per Ni^{2+} . $I(\mathbf{Q}, \omega)$ is the convolution of the cross-section with the resolution function. The solid lines are the scattering expected for the given distribution of chain lengths and convoluted with the resolution function. The nominally pure sample, Y_2BaNiO_5 , ($m = 0.7$ g) was studied using BT4 with $40'-40'-40'-80'$ collimation, a final energy $E_f = 14.7$ meV and a PG filter in the scattered beam. The experiments on the doped sample, $\text{Y}_2\text{BaNi}_{0.96}\text{Mg}_{0.04}\text{O}_5$, ($m = 0.6$ g) were performed using BT2 with the collimation set to $60'-40'-40'-80'$, the final energy $E_f = 13.7$ meV and a PG filter after the sample. Intensities were normalized using the integrated intensity of a transverse acoustic phonon close to the (200) reciprocal lattice point.

tion was fixed at $x = 0.04$.

The only adjustable parameter was a common overall scale factor, which in the single mode approximation is proportional to the ground state energy. The Haldane gaps Δ_∞^α and the mode velocity v_s were fixed at the values measured in the undoped compound [12]. This yields $\langle \mathcal{H} \rangle / L = -1.45(0.4)J$, consistent with numerical results [6]. The excellent agreement between experiment and model in Fig. 1 validates the assumptions made above. In particular the model accurately reproduces the increase of the average gap with impurity concentration x - and thus provides support for upward renormalization of the gap in accordance with $\Delta(L)$.

We have thus far concentrated on the effects of impurities at energies near the Haldane gap Δ of the pure compound. To introduce what occurs at much lower energies, we recall that beyond the triplet excitations above Δ , the AKLT model predicts the existence of a pair of localized composite $S=\frac{1}{2}$ degrees of freedom towards the ends of finite length $S=1$ chains. These are coupled via an indirect exchange interaction $K(L) = (-1)^L 0.8064J \exp(-(L-1)/\xi)$ [17], so that a doped $S=1$ chain system can be described as a set of dimers with a broad distribution of ferro- and antiferromagnetic interdimer couplings. The ground state of a chain segment is a singlet when L is even and a triplet when L is odd. For chains that are much longer than the Hal-

dane length the gap between these levels is much smaller than the Haldane gap. A magnetic field, H , splits the triplet state and inelastic neutron scattering can then be used to probe transitions between quantum states of the nanometer-scale chain segments.

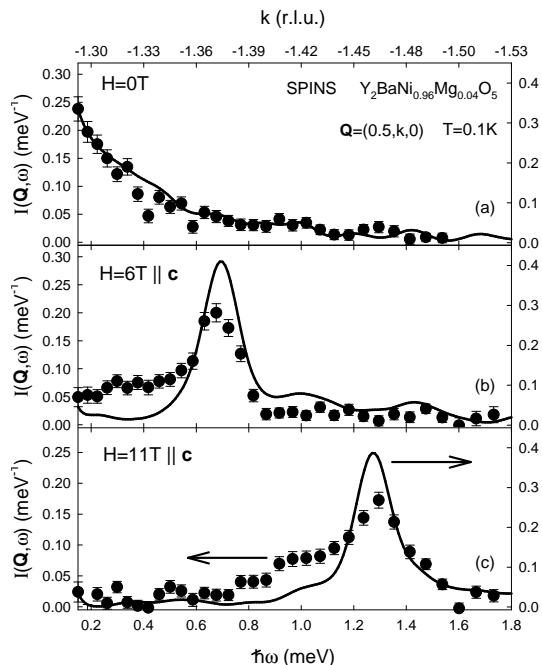


FIG. 2: Spectra at $\mathbf{Q} = (0.5, k, 0)$ for three different fields along the c axis in absolute units (left axis). The solid line is the model described in the text in absolute units (right axis), scaled so that the model matches the scattering at zero field. The top scale shows the median wave-vector transfer in the transverse direction which was varied to maintain \mathbf{k}_f parallel to the chain direction for optimal focusing. The experiment was performed with beam divergences $40'$ - $80'$ - $52'$ - $300'$ for each of the 11 analyzer blade channels, which were set to reflect $E_f = 3.7$ meV to the center of the detector. A BeO filter rejected neutrons with energies higher than 3.7 meV from the detection system. Normalization of the intensity relied on the incoherent elastic scattering from the sample.

The consideration of the coupled chain end states suggests searching for excitations with much lower energies than the Haldane gap. While such excitations cannot exist in pure chains, they should appear in diluted chains at energies of order the indirect exchange interactions, and will yield an inelastic tail extending into the gap from $\hbar\omega = 0$, where the chain end states would reside if the couplings between them were to vanish. Fig. 2a shows that as expected, this phenomenon occurs for $\text{Y}_2\text{BaNi}_{0.96}\text{Mg}_{0.04}\text{O}_5$. To obtain the spectrum displayed, scattering at $(0.4, k, 0)$ and $(0.6, k, 0)$ was averaged and then subtracted as background. For finite fields the spin fluctuations, including those hidden by elastic incoherent scattering should be Zeeman-shifted. Our data also agree with this expectation - the neutron

spectra at $\mathbf{Q} = (0.5, k, 0)$ (Fig. 2b and c) show a well-defined excitation, centered at the Zeeman energy, with clear low energy sidebands.

The data in Fig. 2 can largely be explained using a model of uncoupled dimers consisting of the composite $S = \frac{1}{2}$ degrees of freedom at the chain ends. To include the spin anisotropies in the system we calculated the neutron spectra using the low-energy Hamiltonian introduced by Batista *et al.* [18]:

$$\begin{aligned} \mathcal{H}_L = & E_L^0 + [J\alpha_L + D\beta_L] |0\rangle\langle 0| \\ & + \gamma_L D S_z^2 + \gamma_L E (S_x^2 + S_y^2) - \mu_B g_z H_z S_z, \end{aligned} \quad (3)$$

where E_L^0 , α_L , β_L , and γ_L were computed by the density-matrix renormalization group technique [18] and $|0\rangle\langle 0|$ is the projection onto the singlet state. \mathbf{S} is the spin operator for the dimer. The effect of the anisotropy parameters $D = -0.039J$ and $E = -0.0127J$ [12] is to split the triplet energy levels.

The neutron scattering cross-section for a dimer is

$$\begin{aligned} \frac{d^2\sigma}{d\Omega dE_f}(L) = & (\gamma r_0)^2 \left(\frac{g}{2} F_{\text{Ni}}(\mathbf{Q})\right)^2 \frac{k_f}{k_i} \sum_{\alpha\beta} \sum_{i,j} (\delta_{\alpha\beta} - \hat{\mathbf{Q}}_\alpha \hat{\mathbf{Q}}_\beta) \\ & F_L^{i*}(\mathbf{Q}) F_L^j(\mathbf{Q}) \sum_{\lambda_L \lambda'_L} p_{\lambda_L} \langle \lambda_L | \exp(-i\mathbf{Q} \cdot \mathbf{R}_i) S_i^\alpha | \lambda'_L \rangle \\ & \langle \lambda'_L | \exp(i\mathbf{Q} \cdot \mathbf{R}_j) S_j^\beta | \lambda_L \rangle \delta(E_{\lambda_L} - E_{\lambda'_L} + \hbar\omega), \end{aligned} \quad (4)$$

where $|\lambda_L\rangle$ denotes the dimer singlet and triplet states with energy E_{λ_L} and population factor p_{λ_L} . The index $i, j = 1, 2$ numbers the composite $S = \frac{1}{2}$ at a position R_i towards the end of the chain and $\alpha, \beta = x, y, z$. We used $g = g_z = 2.165$ as determined from ESR [18] and $(\gamma r_0)^2 = 0.29$ barn. $F_L^i(\mathbf{Q})$ is the form factor of the end-chain composite spin and describes the decaying AF magnetization at the chain ends associated with the collective spin degree of freedom. We will give an experimental view of this quantity below; for the moment, we simply assert that its square is well described by a normalized Lorentzian centered at $h = 0.5$ with a width Γ given by $\Gamma^2 = (\frac{1}{\xi^2} + \frac{1}{L^2})/\pi^2$. This should be a good approximation because the Fourier transform of an exponentially decaying correlation function for the staggered magnetization is a Lorentzian, and the finite length L of the chain acts as a finite size cutoff.

The scattering cross-section for a given dimer distribution was obtained by adding contributions from all chain segment lengths $\frac{d^2\sigma}{d\Omega dE} = \sum_L P(L, x) \frac{d^2\sigma}{d\Omega dE}(L)$ and convoluting with a Gaussian to account for the finite energy resolution. Lacking detailed singlet and triplet wave functions for a chain segment, interference effects, such as the twin incommensurate peaks for the subgap bound states in hole-doped $\text{Y}_{2-x}\text{Ca}_x\text{BaNiO}_5$ [3], between chain ends were ignored. This should be a good approximation for an ensemble of long chains. The solid line in Fig. 2 shows the absolute scattering intensity expected from this model. The weakly oscillatory nature of the calculated spectrum follows from the discrete nature of the

distribution of indirect exchange couplings $K(L)$. At zero field there is excellent agreement between experiment and theory with an 28% adjustment of the pre-factor (within the 30% error bar from normalization) being the only adjustable parameter. At finite field the model reproduces the position of the well-defined peak ($g_z = 2.0(0.05)$ gives a slightly better fit than $g_z = 2.165$ from ESR [18]) but it overestimates its intensity, which seems to be transferred to a continuum that cannot be accounted for by the model. The broad scattering below the well-defined excitation indicates that changes in the chain end structure with field or interchain coupling play an important role. If interchain interactions indeed couple the chain segments then the doped sample may eventually freeze into a low-temperature AF or spin glass state.

Neutron scattering has the tremendous advantage of providing spatial as well as spectral information about spin fluctuations. We have thus examined the form factor for the edge states at the Zeeman energy by scanning wave vector h with fixed $\hbar\omega$. Fig. 3 shows the result. Rather than a broad maximum centered at $h = 0$ corresponding to the form factor for a localized atomic spin, we find a relatively sharp peak centered at $h = 0.5$. This is direct evidence that chain end spins carry AF spin polarization back into the bulk of the chain segments. By fitting the model cross-section (Eq. 4) convoluted with the resolution function to the data we find the exponential decay length ξ for the chain-end staggered spin density (inset of Fig. 3). The decay length remains constant at $\xi = 8(1)$ between $H = 4$ and 11 T - in perfect agreement with the equal-time correlation length $\xi = 8(1)$ for undoped Y_2BaNiO_5 in zero field at low temperatures $T/J \ll 1$ [19], but slightly longer than that deduced from an NMR study of the staggered magnetization [8]. A fit to a square-root Lorentzian, which would be appropriate for unpinned (by impurities) bulk spin correlations from the Haldane continuum, yields a longer correlation length $\xi = 13(1)$. Note that because we have fixed $\hbar\omega$ at precisely the Zeeman energy, we have maximized the contribution of those chains with the smallest coupling and hence largest lengths to the scattering, thus revealing $F_{L \approx \infty}^i(\mathbf{Q})$, in the notation of Eq. 4.

In summary, our inelastic neutron scattering experiment on Mg-doped Y_2BaNiO_5 shows an upward renormalization of the Haldane gap with doping, which is consistent with numerical predictions for a distribution of finite chain segments. In addition, we find well-defined excitations below the Haldane gap whose field dependence demonstrates that they originate from $S = \frac{1}{2}$ chain-end degrees of freedom. Their wave-vector dependence shows chain end states carry an AF "Friedel" oscillation that extends into the chain segment with an exponential decay length $\xi = 8(1)$ in a field $H = 11$ T. The experiment also demonstrates a new technique, neutron ESR, by which the structure of composite spin degrees of freedom liberated from a macroscopic singlet can be probed. Efforts

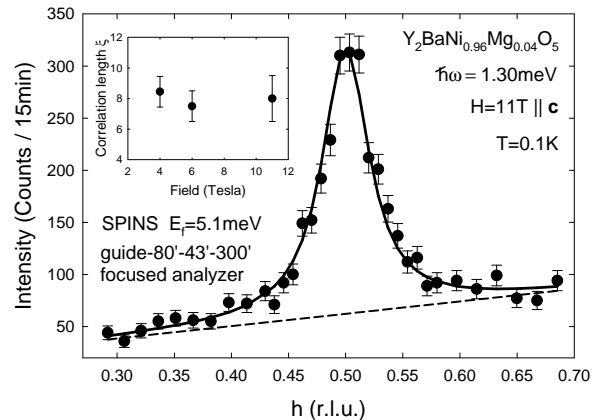


FIG. 3: Scattering originating from $S = \frac{1}{2}$ chain end states at the resonance energy $\hbar\omega = 1.30$ meV for $H = 11$ T (applied along the c axis) in $\text{Y}_2\text{BaNi}_{0.96}\text{Mg}_{0.04}\text{O}_5$ as a function of h . The solid line is a fit explained in the text and the dashed line is the background. Inset: Correlation length ξ as a function of field. For this experiment $E_f = 5$ meV and there was a cooled Be filter in the scattered beam.

are now underway to apply this approach to understand impurity structure and dynamics in more complex systems such as high-temperature superconductors [20].

We thank C. D. Batista for sending us numerical results. Work at JHU was supported by the NSF through Grant No. DMR-0074571. Work at LSU was supported through Grant No. DMR-0103892. Work at BNL was supported by DOE Division of Materials Sciences under Contract DE-AC02-98CH10086. The work at SPINS was supported by NSF through DMR-9986442. The high-field magnet used was funded in part by NSF through DMR-9704257.

-
- [1] S. H. Pan *et al.* Nature **403**, 746 (2000).
 - [2] E. W. Hudson *et al.* Nature **411**, 920 (2001).
 - [3] G. Y. Xu *et al.* Science **289**, 419 (2000).
 - [4] F. D. M. Haldane, Phys. Rev. Lett. **50**, 1153 (1983).
 - [5] I. Affleck *et al.* Phys. Rev. Lett. **59**, 799 (1987).
 - [6] S. R. White *et al.* Phys. Rev. B **48**, 3844 (1993).
 - [7] S. H. Glarum *et al.* Phys. Rev. Lett. **67**, 1614 (1991).
 - [8] F. Tedoldi *et al.* Phys. Rev. Lett. **83**, 412 (1999).
 - [9] A. P. Ramirez *et al.* Phys. Rev. Lett. **72**, 3108 (1994).
 - [10] D. J. Buttrey *et al.* J. Solid State Chem. **88**, 291 (1990).
 - [11] T. Ito *et al.* Phys. Rev. B **64**, 060401(R) (2001).
 - [12] G. Xu *et al.* Phys. Rev. B **54**, R6827 (1996).
 - [13] J. F. DiTusa *et al.*, Phys. Rev. Lett. **73**, 1857 (1994).
 - [14] E. S. Sorensen *et al.* Phys. Rev. Lett. **71**, 1633 (1993).
 - [15] S. Ma *et al.* Phys. Rev. Lett. **69**, 3571 (1992).
 - [16] N. J. Chesser and J. D. Axe, Acta Cryst. **A29**, 160 (1973).
 - [17] E. S. Sorensen *et al.* Phys. Rev. B **49**, 15771 (1994).
 - [18] C. D. Batista *et al.*, Phys. Rev. B **60**, R12553 (1999).
 - [19] Y. Chen *et al.*, to be published.
 - [20] B. Lake *et al.*, Science **291**, 1759 (2001).